

Evidence of fibril-like β -sheet structures in a neurotoxic amyloid intermediate of Alzheimer's β -amyloid

Sandra Chimon, Medhat A Shaibat, Christopher R Jones, Diana C Calero, Buzulagu Aizezi & Yoshitaka Ishii

Diffusible subfibrillar aggregates of amyloid proteins are potent neurotoxins and primary suspects in amyloid diseases including Alzheimer's disease. Despite widespread interest, the molecular structures of the amyloid intermediates and the conformational conversions in amyloid misfolding are poorly understood. Here we present a molecular-level examination of sequence-specific secondary structures and supramolecular structures of a neurotoxic amyloid intermediate of the 40-residue β -amyloid ($A\beta$) peptide involved in Alzheimer's disease. Using solid-state NMR and electron microscopy, we show that, before fibrillization, natively unstructured monomeric $A\beta$ is subject to large conformational changes into a spherical amyloid intermediate of 15–35 nm diameter, which has predominantly parallel β -sheet structures. Structural comparison with $A\beta$ fibrils demonstrates that formation of this β -sheet intermediate (I_β) largely defines conformational transitions in amyloid misfolding. Neurotoxicity assays on PC12 cells show that I_β shows higher toxicity than the fibril, indicating that the β -sheet formation may trigger neurotoxicity.

Amyloid diseases are a group of progressive disorders including Alzheimer's disease, Parkinson's disease and prion diseases, many of which lack effective cures. These amyloid diseases are commonly characterized by misfolding of disease-specific amyloid proteins, leading to self-assembled fibrillar aggregates^{1,2}. Because amyloid-forming proteins across diverse systems show common structural and kinetic characteristics after fibril formation, it has been speculated that different amyloid diseases may share a common molecular mechanism^{3–5}. Notably, many amyloid proteins, which are nontoxic in monomeric forms, show cytotoxicity after fibrillization. Thus, toxicity and neurodegeneration in amyloid diseases have long been attributed to amyloid fibrils^{1,6}. Some studies, however, have identified morphological variants of diffusible subfibrillar aggregates during misfolding of amyloid proteins^{2,7–12}. More interestingly, some of these diffusible amyloid intermediates show much higher toxicity than fibrils^{2,8,9}.

Human Alzheimer's $A\beta$ peptides (39–43 residues) self-assemble into amyloid fibrils, which are a primary component of amyloid plaques—a pathological hallmark of the brain in Alzheimer's disease. Intensive studies of amyloid intermediates, and in particular of $A\beta$, have revealed strong links between amyloid intermediates and amyloid disease. For example, some pathogenic mutations in $A\beta$ and in α -synuclein (which is associated with Parkinson's disease) promote the formation of amyloid intermediates rather than fibrils^{10–12}. It has been reported that dysfunction of neurons does not correlate well with the distribution and density of fibrils in affected humans and mouse models of Alzheimer's disease; rather, the amount of soluble $A\beta$, which includes diffusible $A\beta$ aggregates, correlates with neural dysfunction^{13–15}. Diffusible $A\beta$ aggregates also inhibit long-term potentiation¹⁶ and disrupt memory¹⁷ in mouse models. Thus, it is

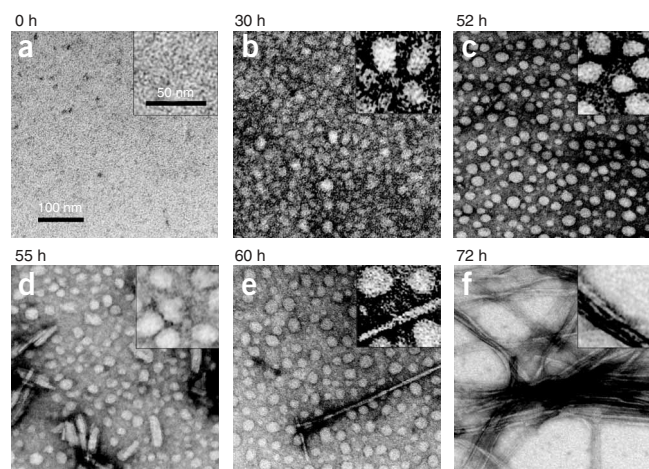
widely considered that amyloid intermediates have a primary role at the onset of amyloid diseases, including Alzheimer's disease and Parkinson's disease^{1,2}.

Structures of amyloid intermediates have attracted broad attention as potential therapeutic targets, particularly at early stages of amyloid diseases. Amyloid intermediate structures also provide insights into the molecular mechanisms of amyloid misfolding and the high neurotoxicity of the intermediate species. Morphologies of the diffusible amyloid aggregates have been identified by transmission electron microscopy (TEM) and atomic-force microscopy^{8,9,18}. Structural changes in amyloid misfolding have been examined by optical spectroscopic methods¹⁸ and chemical cross-linking¹⁹. By contrast, the intrinsic instability and noncrystallinity of the systems have long prohibited molecular structural studies of amyloid intermediates with site-specific resolution. For amyloid proteins with native folds, solution NMR and X-ray crystallography studies have shown that partially unfolded states may trigger misfolding into fibrils^{20–22}. For β 2 microglobulin, for example, two studies have independently identified molecular structures of monomeric and dimeric amyloid intermediates that largely retain a native structure^{21,22}. These small native-like intermediates probably correspond to the first stage toward misfolding into fibrils²³. Indeed, increasing evidence suggests that amyloid intermediates exist that are larger than small oligomers, and that the later-stage aggregates have higher toxicity^{2,7–12,24}. It is highly probable that the formation of these larger intermediates involves more profound conformational transitions toward amyloid fibrils²³. However, there have been few molecular structural studies on the later-stage amyloid intermediate species, which may fill a missing link in the structural transition from monomeric proteins to amyloid fibrils.

Department of Chemistry, University of Illinois at Chicago, Chicago, Illinois 60607, USA. Correspondence should be addressed to Y.I. (yishii@uic.edu).

Received 11 August 2006; accepted 1 November 2007; published online 2 December 2007; doi:10.1038/nsmb1345

Figure 1 Morphological properties of A β_{1-40} aggregates after different incubation periods (*t*). (a–f) Dependence on *t* of TEM images of a 100 μ M solution of A β_{1-40} , which was incubated at 4 °C and pH = 7.4 \pm 0.1 and sampled at *t* = 0 h (a), 30 h (b), 52 h (c), 55 h (d), 60 h (e) and 72 h (f). Spherical intermediates were observed in b–e and isolated in c. Protofibrils, resembling truncated fibrils, were observed in d. The buffer contained 5 mM NaCl, 10 mM phosphate and 0.02% NaN₃.



We have investigated sequence-specific secondary structures and supramolecular structures of a neurotoxic amyloid intermediate observed at the late stage of amyloid misfolding of a 40-residue A β peptide, A β_{1-40} , by using solid-state NMR (SSNMR) and TEM. On the basis of the structural information obtained, we have examined whether substantial structural transitions precede fibril formation in amyloid misfolding of the full-length A β . In addition, we have assessed the kinetics of formation of the amyloid intermediate in the presence of the seeded intermediate species by fluorescence spectroscopy using thioflavin T (ThT), a quantitative indicator of β -sheet-rich aggregates. The results suggest that two kinds of diffusible intermediates with notably distinctive conformations exist. We present a possible molecular kinetic model of amyloid misfolding, based on our structural and kinetic data, that offers clues to therapeutic strategies targeted to amyloid intermediates. Our study provides encouraging prospects for the molecular structural characterization of other amyloid intermediates.

RESULTS

Morphological evolution in A β misfolding

We examined the dependence on incubation time (*t*) of negatively stained TEM images of a 100 μ M solution of A β_{1-40} (Fig. 1). No visible structures were observed by TEM at *t* = 0 (Fig. 1a), consistent with the existence of monomers (or small oligomers), after filtration of the solution with a filter with a 50-kDa molecular weight cutoff (MWCO). By contrast, we observed spherical intermediates of 15–35 nm in diameter that were stabilized at 4 °C at *t* = 30–60 h (ref. 25 and Fig. 1b–e). In particular, well-defined homogeneous spheres were observed as the dominant species at *t* = 52 h. The spherical morphologies observed resembled those of previously reported intermediate species such as A β -derived diffusible ligand (ADDL)⁸ and amylospheroid⁹. The average diameter of our intermediate (15–35 nm) was comparable to that of the spheroid (8–16 nm) and much larger than that of ADDL (~5 nm). As we discuss later, however, the spherical intermediate contained extended β -sheet structures, as detected by ThT fluorescence²⁵, whereas amylospheroids do not show ThT fluorescence. Thus, it seemed likely that our spherical intermediate was a new intermediate species.

At 72 h, the fibrils became the dominant species (Fig. 1f). During the transition period, protofibrils^{2,7} (Fig. 1d), which resemble truncated fibrils, and long fibrils (Fig. 1e) were observed with the spheres. The spherical intermediate species was identified by TEM in the top 70% of the supernatant after centrifugation for 15 min at 13,200g, whereas the protofibrils and fibrils were in the bottom 30%. Similar results were obtained when a 50 μ M solution of A β_{1-40} was used (Supplementary Fig. 1 online). This finding clearly suggests that the observed spherical intermediate is a diffusible intermediate species and can be distinguished from protofibrils and fibrils by both this physical property and the morphologies observed by TEM.

Neurotoxicity of the late-stage amyloid intermediate

We next examined the concentration dependence of neurotoxicity of the intermediate collected at *t* = 52 h, together with the corresponding

toxicity of matured fibrils and monomers (Fig. 2). The toxicity on PC-12 cells was evaluated by a standard MTT assay²⁶. The monomer sample was collected at *t* = 0 h, whereas the fibril sample was collected after 7 d incubation at 4 °C. We found that the concentration of the intermediate needed to inhibit 50% of cell viability (IC₅₀) was less than 1 μ M. The IC₅₀ value of the spherical intermediate was at least ten-fold lower than that of the matured fibrils (~10 μ M), indicating that the intermediate has markedly higher neurotoxicity. As reported previously, the monomer showed no or minimal toxicity^{6,9}.

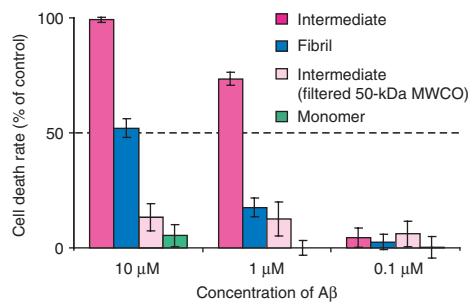
To evaluate the toxicity of small oligomers that might coexist with the spherical intermediate shown in Figure 1c, we tested the toxicity of the solution sampled at *t* = 52 h after filtering it with a 50-kDa-MWCO filter (Fig. 2). Only minimal toxicity was observed for the filtered sample containing monomers and small oligomers. TEM analysis confirmed that the filtered solution did not contain the spheres observed in Figure 1c. Thus, it is likely that the spherical intermediate species observed in Figure 1c is responsible for the high neurotoxicity.

A preliminary neurotoxicity inhibition assay using the A11 antibody, which inhibits the toxicity of some earlier-stage intermediates of A β (ref. 27), showed only minor or no inhibition of the toxicity of the spherical intermediate species (Supplementary Fig. 2 online) and no inhibition of the toxicity of the fibril. A glycerol gradient sedimentation assay suggested that the spherical species of 10–35 nm, which was identified in TEM images of the two bottom fractions, has a molecular weight of 650 kDa (150 monomers) or higher (Supplementary Fig. 3 online). Additional toxicity assays for the aggregates separated by the sedimentation assay confirmed that high toxicity was associated with the larger spherical species rather than the smaller aggregates (see Supplementary Fig. 3).

The intermediate has ordered β -sheet structures

We considered that structural insights into the neurotoxic amyloid intermediate of A β_{1-40} and the molecular kinetics in amyloid misfolding could be obtained by examining the detailed molecular and supramolecular structure of the intermediate by SSNMR using techniques that have been applied to the thermally stable amyloid fibrils^{28–33} and other proteins^{34–37}. Structural analysis by SSNMR usually requires a homogeneous sample, which has been difficult to prepare for amyloid intermediates. Because we could successfully isolate a reasonably homogeneous amyloid intermediate (Fig. 1c) showing notable neurotoxicity, we used this intermediate for molecular structural analysis. To trap the thermally unstable intermediate,

Figure 2 Toxicity of $A\beta_{1-40}$ monomers, intermediates and fibrils assessed by MTT assay. Shown is the dependence of neurotoxicity (% cell death as compared to control) on the concentration of $A\beta_{1-40}$ in different morphologies on PC-12 neural cells, as measured by MTT assay. $A\beta_{1-40}$ aggregates are expressed as a monomer-equivalent concentration, which was estimated from the concentration of the original $A\beta_{1-40}$ solution (100 μM) coupled with dilution factors (10^1 – 10^3). For the filtered sample, the original concentration of 100 μM before filtration was divided by a factor of 10^1 – 10^3 for comparison. Cell activity was optically measured as reduction of the MTT dye by viable cells after a 4-h exposure to $A\beta_{1-40}$. A negative control sample was lysed with Triton X-100 to examine the relative mortality rate of the PC-12 cells treated with $A\beta_{1-40}$ sampled at various incubation times. Data are the mean of four trials and three separate cell lines for each condition relative to the controls. Error bars denote 1.8 times the s.d. of the mean in the cell death rate (or 90% confidence interval). The intermediate, which was sampled at $t = 52$ h, showed the highest toxicity. By contrast, $A\beta_{1-40}$ solution sampled at $t = 0$ ('monomer') showed no toxicity. A filtrate of the 52-h sample (50-kDa MWCO) showed minimal toxicity, even at 10 μM .



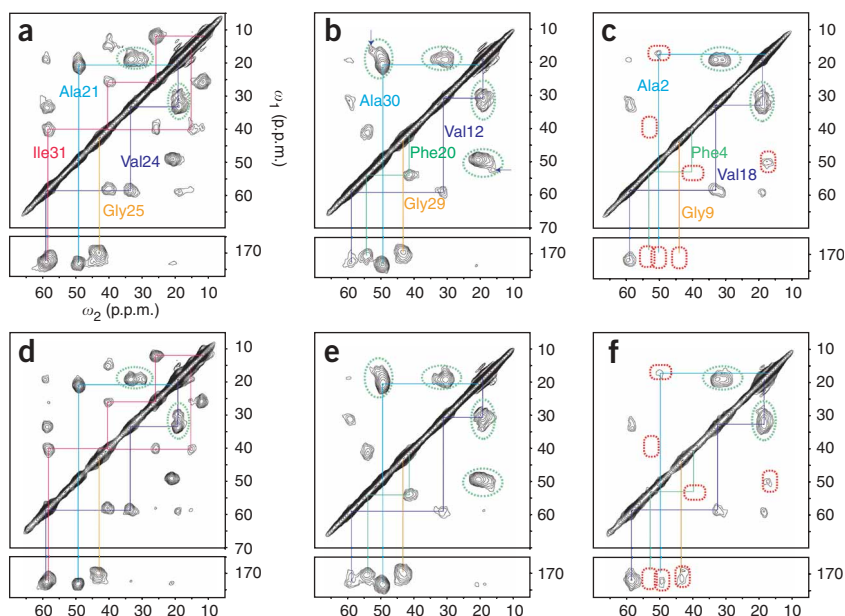
we used freeze-trapping and subsequent lyophilization²⁵, and then analyzed the lyophilized samples by SSNMR. Various proteins including $A\beta$ in fibrils retain their structures after lyophilization^{29,33,38}. We confirmed that the spherical morphology of the lyophilized intermediates after rehydration was nearly identical to that before lyophilization (Supplementary Fig. 4 online) and that lyophilization did not alter the kinetic pathway of $A\beta$ misfolding detected by ThT fluorescence (Supplementary Fig. 5 online).

We compared the two-dimensional (2D) ^{13}C - ^{13}C chemical shift correlation SSNMR spectra for the spherical intermediate (Fig. 3a–c) and the fibril (Fig. 3d–f) using three different labeling schemes with uniform ^{13}C and ^{15}N labeling at Ala21, Val24, Gly25 and Ile31 (Fig. 3a,d); Val12, Phe20, Gly29 and Ala30 (Fig. 3b,e); and Ala2, Phe4, Gly9 and Val18 (Fig. 3c,f). Although the intermediate samples also contained monomeric or small oligomeric $A\beta$, the ^{13}C SSNMR signals for these species were negligible, presumably because of considerable line broadening resulting from structural disorder in the unstructured monomeric species²⁵ (Supplementary Fig. 6 online). The positions of shifts sensitively reflect conformations at specific residues^{29–31,39–41}; thus, distribution of the ^{13}C shift (that is, linewidth) provides information on structural order²⁹. Except for those of residues in the N terminus (Ala2, Phe4 and Gly9) and a few other resonances,

the linewidths were generally narrow (2–3 p.p.m.) for the intermediate (Fig. 3a–c), considering the fact that noncrystalline lyophilized samples were used and that the linewidths included ^{13}C - ^{13}C J couplings (~ 0.5 p.p.m.) and gaussian broadening (1 p.p.m.). The linewidths for the intermediate were comparable to those for fibrils, which are known to be structurally well ordered²⁹. This finding suggests that, despite the size variation observed in Figure 1c, the intermediate has well-ordered structures. The shifts of our intermediate and the fibrils were similar despite the morphological differences.

As mentioned above, signal intensities for the N-terminal residues (Ala2, Phe4 and Gly9) were low (Fig. 3c), suggesting line broadening owing to considerable structural disorder at the N-terminal regions in the intermediate species. By contrast, the signals for Val18 in the hydrophobic core region were much stronger (Fig. 3c), indicating that this residue has a well-ordered structure. A similar trend was observed for the fibril sample (Fig. 3f), which suggests that the unstructured region in the intermediate is preserved in the fibrils. We found that the cross peaks between $C\alpha$ and $C\beta$ and those between $C\beta$ and $C\gamma$ of Val12 were reasonably strong and sharp (linewidth ≈ 3 p.p.m.) for the intermediate, although broader peaks (~ 5 p.p.m.) were observed for the CO region (Fig. 3b). Thus, disorder is likely to be restricted to the first ten residues in the N-terminal. Although attenuated signals for

Figure 3 Comparison of SSNMR data for the amyloid intermediate and the fibril. (a–f) 2D ^{13}C - ^{13}C correlation SSNMR spectra obtained with the fpRFDR sequence and a mixing time of 1.6 ms for amyloid intermediate (a–c) and fibril (d–f) samples of $A\beta_{1-40}$ with uniformly ^{13}C and ^{15}N labeling at Ala21, Val24, Gly25 and Ile31 (a,d); Val12, Phe20, Gly29 and Ala30 (b,e); and Ala2, Phe4, Gly9, Val18 (c,f). Color-coded lines denote signal assignment for glycine (yellow), alanine (light blue), valine (dark blue), phenylalanine (green) and isoleucine (red). See Supplementary Methods and Supplementary Data online for experimental details and assignments. The fibrils were collected as a precipitate after centrifugation to minimize contamination from monomers and other diffusible aggregates. Broken green circles denote multiple peaks corresponding to the same resonance; broken red circles denote missing or weak cross peaks, presumably due to structural disorder. In each spectrum, the lowest contour level was set to 7% of the diagonal peak of $^{13}\text{C}\alpha$ of Ala (a,d) or Val (b,c,e,f), which was well resolved from other diagonal peaks.



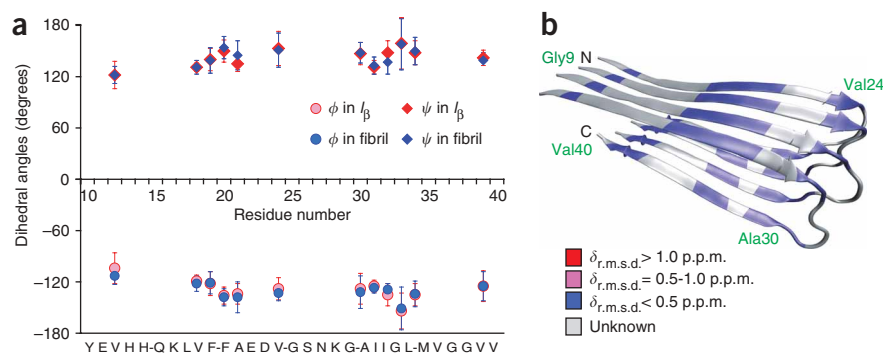


Figure 4 Conformation and ^{13}C chemical shift analyses of I_β and fibril by SSNMR. **(a)** Dihedral angles (ϕ , ψ) of $\text{A}\beta_{1-40}$ estimated by TALOS analysis for I_β and fibrils. The first ten residues in the N terminus were omitted because of line broadening owing to substantial structural disorder. The angles indicate the mean values of the corresponding angles for the ten protein fragments that showed best matches between ^{13}C solution NMR shifts⁴⁴ and the present ^{13}C SSNMR data; the color-coded error bars denote the s.d. of the angles. **(b)** The ^{13}C $\delta_{r.m.s.d.}$ between I_β and fibrils for different residues. The color-coded $\delta_{r.m.s.d.}$ for the residues are mapped on a structural model of $\text{A}\beta_{1-40}$ fibrils⁴⁵ lacking the first eight residues in the N terminus. For glycine residues, $\delta_{r.m.s.d.} = [(\delta(^{13}\text{C}\alpha)^2 + \delta(^{13}\text{CO})^2)/2]^{1/2}$; for other residues, $\delta_{r.m.s.d.} = [(\delta(^{13}\text{C}\alpha)^2 + \delta(^{13}\text{C}\beta)^2 + \delta(^{13}\text{CO})^2)/3]^{1/2}$, where $\delta(X)$ denotes the chemical shift difference between I_β and fibril for the resonance $^{13}\text{C}\alpha$, $^{13}\text{C}\beta$ or ^{13}CO .

Gly38 and Val39 in the C terminus (data not shown) were observed, the signals were still visible for these residues. Thus, structural disorder in the C terminus is probably minimal.

I_β predefines fibril conformations in misfolding

We identified multiple peaks assigned to common resonances, particularly for $^{13}\text{C}\alpha$ and $^{13}\text{C}\beta$ of Ala30 and $^{13}\text{C}\beta$ of Val12, Val18 and Val24, in both the intermediate and the fibril (Fig. 3). These multiple peaks support the coexistence of multiple conformers or polymorphologies^{31,42}. The ratios of the peak intensities of the ‘multiplets’ differed from residue to residue. For the intermediate species, for example, there were two major cross peaks between $^{13}\text{C}\alpha$ and $^{13}\text{C}\beta$ of Ala30 (Fig. 3b). Whereas the shifts of the stronger peaks for Ala30 at 49.3 p.p.m. (ω_1) and 20.8 p.p.m. (ω_2) correspond to β -sheet (referenced to TMS), those of the weaker peaks at 52.6 p.p.m. (ω_1) and 16.3 p.p.m. (ω_2) suggest α -helical structures^{39,40}; by contrast, the reported random-coil chemical shifts are 50.8 p.p.m. (ω_1) and 17.4 (ω_2) p.p.m. for $^{13}\text{C}\alpha$ and $^{13}\text{C}\beta$, respectively, in the TMS reference⁴³. Although more quantitative analysis is required, these observations imply the existence of an amyloid intermediate incorporating helical structure as a minor conformer. A previous circular dichroism study also supports the existence of an intermediate containing α -helical structures¹⁸. Because the corresponding minor cross peaks in amyloid fibrils were considerably weaker, the minor conformer may be a unique characteristic of the amyloid intermediate.

For $^{13}\text{C}\beta$ of Val12, Val18 and Val24, we observed two peaks at ~ 31 and ~ 33 p.p.m. The relative intensity ratio and the peak positions of the multiple peaks, which varied among the residues, were nearly identical in both fibril and intermediate for each residue. It is unlikely that the minor peaks in the fibril or intermediate samples were due to contaminants. For the fibril sample used in the SSNMR experiments, we collected only precipitates obtained after centrifugation, and these precipitates comprised only 3% of the total solution volume; thus, contamination from soluble species would be negligible. For the intermediate sample, very weak ^{13}C SSNMR signals were observed for the sample that was prepared by first filtering the $\text{A}\beta_{1-40}$ solution at $t = 52$ h with a 50-kDa-MWCO filter and then lyophilizing

the filtrate (Supplementary Fig. 6d); thus, the contribution of small oligomers or monomers in the spectra of the intermediate (Fig. 3a–c) should be minor. In addition, for most other resonances, we found a relatively narrow single peak for each cross peak. Thus, the data strongly suggest that multiple conformers in relatively similar β -sheet structures are shared by the intermediate and the fibril. The existence of multiple conformers in the fibrils is consistent with previous SSNMR studies on $\text{A}\beta_{1-40}$ fibrils⁴². Because these data show that formation of the intermediate precedes that of the fibrils, we conclude that the multiple conformers are first formed in the intermediate and that the intermediate structures define the structures of the multiple conformers in fibrils in amyloid misfolding.

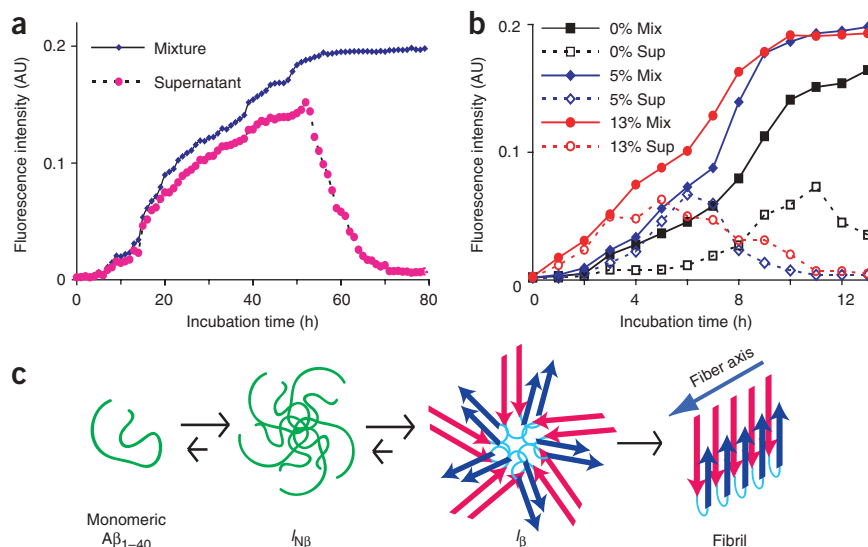
To compare structures of the fibril and the intermediate more quantitatively, we elucidated the backbone dihedral angles (ϕ , ψ) on the basis of the ^{13}C shifts by using TALOS analysis⁴⁴. We analyzed only the strongest

cross peak when multiple cross peaks were observed; thus, this analysis provided structural information on the primary conformer. The ϕ and ψ backbone torsion angles estimated for the spherical intermediate and fibrils clearly suggested that the structure of the intermediate is dominated by β -sheet (Fig. 4a). On the basis of these results, we called the spherical intermediate species the ‘ β -sheet intermediate’ (I_β). Structures were not reported for Gly25 and Gly29, which may be involved in the formation of a loop region identified in $\text{A}\beta_{1-40}$ fibrils²⁹.

The dihedral angles and the suggested β -sheet regions were nearly identical between fibrils and I_β (Fig. 4a). The suggested β -sheet regions in the fibril were consistent with previous studies^{29,42}, although there were considerable differences in ^{13}C chemical shifts, which may suggest minor structural differences owing to polymorphisms⁴². We compared the ^{13}C chemical shifts between the major I_β species and the fibril mapped on a structural model of $\text{A}\beta_{1-40}$ fibril⁴⁵ (Fig. 4b). The shifts were surprisingly similar between the two species: the r.m.s. deviations of the ^{13}C shifts ($\delta_{r.m.s.d.}$) between the I_β and fibril for $^{13}\text{C}\alpha$, $^{13}\text{C}\beta$ and ^{13}CO were within 0.5 p.p.m. for all residues examined. The observed difference was relatively small as compared with the estimated measurement error (of about ± 0.2 p.p.m.). Thus, this result again supports the idea that the conformations of the amyloid fibrils are defined by those of I_β , at least at the level of secondary structure.

We also determined the interstrand distance in two $\text{A}\beta_{1-40}$ samples labeled at ^{13}CO of Ala21 or Ala30 for I_β and fibrils by measuring the interstrand ^{13}C – ^{13}C direct dipolar couplings with a constant-time finite-pulse radiofrequency-driven recoupling (fpRFDR-CT) sequence^{29,41}. Comparison of experimental and simulated dipolar dephasing curves (Supplementary Fig. 7 online) suggested interstrand ^{13}CO – ^{13}CO distances at these sites of 0.59 ± 0.02 and 0.60 ± 0.02 nm for I_β and fibrils, respectively. The distances obtained suggest that both I_β and fibril have in-register parallel β -sheet structures⁴². Although we measured only two interstrand distances, previous SSNMR studies of $\text{A}\beta$ fibrils suggest that longer $\text{A}\beta$ peptides including $\text{A}\beta_{1-40}$ and $\text{A}\beta_{10-35}$ form parallel β -sheets^{29,33}. Thus, on the basis of the interstrand distances obtained for I_β and the similarity in the ^{13}C chemical

Figure 5 Kinetic properties of I_β formation assessed by ThT fluorescence and I_β seeding experiments. **(a)** Dependence of ThT fluorescence on t for a 100 μM solution of $\text{A}\beta_{1-40}$ incubated at 4 $^\circ\text{C}$. Before sampling 25 μl of $\text{A}\beta$ solution for each analysis, the solution was gently mixed (mixture) or an aliquot was removed and centrifuged for 15 min at 13,200g (supernatant). The incubation conditions were the same as in **Figure 1**. **(b)** Dependence on I_β seeding of buildup curves of the ThT fluorescence intensity for the mixture and the supernatant with no seeding, 5% seeding and 13% seeding of I_β at 25 $^\circ\text{C}$. The fluorescence buildup occurs earlier with I_β seeding. The lag time in **b** without seeding (~ 3 h) is substantially shorter than that in **a** (~ 8 h) because of the higher temperature, which promotes fibril formation; 13% seeding further reduces the lag time in **b**. **(c)** Kinetic model suggested by the SSNMR and ThT fluorescence experiments.



shifts between the fibril and I_β , it seems likely that I_β forms parallel β -sheet structures. In protein folding, many proteins fold into metastable intermediates that possess native-like secondary structures before the transition into native folds. Our results suggest that $\text{A}\beta_{1-40}$ also misfolds into an intermediate state that has well-defined fibril-like parallel β -sheet structures (secondary structure) but with only a metastable supramolecular packing (tertiary structure) before final fibrillization. Because the conformations suggested by SSNMR are similar between I_β and fibrils, the high toxicity of I_β may be attributed to the unique supramolecular structures of I_β in addition to the conformational changes of $\text{A}\beta_{1-40}$.

Two-step misfolding of $\text{A}\beta_{1-40}$ suggested by ThT fluorescence

To identify the kinetic pathway of misfolding of $\text{A}\beta_{1-40}$, we examined β -sheet formation by using ThT fluorescence, a quantitative indicator of the formation of amyloid aggregates with β -sheet structures^{25,46}. The ThT assay is insensitive to many globular β -sheet-containing proteins, which typically contain short stretches of β -sheet structures⁴⁶. We measured the dependence of ThT fluorescence on t for a 100 μM solution of $\text{A}\beta_{1-40}$ incubated at 4 $^\circ\text{C}$ (**Fig. 5a**; see **Supplementary Fig. 1** for experiments on a 50 μM solution). The reduced temperature stabilizes formation of the diffusible intermediate species. The fluorescence increased in a sigmoidal manner after a lag time⁴⁷, indicating the formation of β -sheet-rich fibrils. To detect soluble intermediate species involving β -sheet structures, we performed a quick centrifugation (15 min, 13,200g) on an aliquot (~ 1 ml) of the $\text{A}\beta_{1-40}$ solution sampled at different values of t and measured the ThT fluorescence of the supernatant collected (**Fig. 5a**). The diffusible β -sheet intermediate, I_β , was clearly observed at $t = 30$ – 52 h, consistent with the TEM images (**Fig. 1**).

We identified a lag time before the formation of I_β (**Fig. 5a**), which excludes the possibility of a direct conversion of monomeric $\text{A}\beta_{1-40}$ to I_β , as we reason in the following. Suppose that only monomers in a random coil state (M_{rc}) exist initially. If I_β is derived directly from n units of M_{rc} as $nM_{rc} \rightarrow I_\beta$, the rate of I_β formation should be given by

$$d[I_\beta]/dt = k[M_{rc}]^n \quad (1)$$

where t denotes the incubation time, and k is a rate constant. Because $[M_{rc}]$ is the highest at $t = 0$, then $d[I_\beta]/dt$ should be maximum at

$t = 0$. It seems that equation (1) is not valid because the slope of the curve for I_β (**Fig. 5a**) is nearly zero at $t \approx 0$. Thus, I_β must be formed from an earlier intermediate species that does not contain amyloid-like β -sheets, which we call a non- β intermediate ($I_{N\beta}$). In other words, the formation of I_β requires a reaction cascade: $M_{rc} \rightarrow I_{N\beta} \rightarrow I_\beta$ (coefficients omitted). Thus, these results suggest that $I_{N\beta}$ lacks extended β -sheets, which are a signature of amyloid aggregates.

An alternative model that can explain the sigmoidal behavior observed in **Figure 5a** is a nucleation mechanism⁴⁷. In this model, the formation of the detected aggregate (I_β in this case) is preceded by the initial slow formation of ‘nuclei’—that is, aggregates that have higher free energy than monomers and I_β . As described later, an I_β seeding experiment showed that I_β may form through the nucleation mechanism⁴⁷, but this mechanism would involve amyloid aggregates corresponding to $I_{N\beta}$.

Seeding of I_β in ThT fluorescence shows reversible formation of I_β

To confirm that I_β is an on-pathway intermediate, we measured the dependence of ThT fluorescence on t in the presence of I_β ‘seeded’ to an $\text{A}\beta_{1-40}$ solution. We reasoned that, if I_β is a key kinetic intermediate, increasing the concentration of I_β by seeding I_β should promote fibril formation. We measured the dependence of ThT fluorescence on I_β seeding for a 100 μM solution of $\text{A}\beta_{1-40}$ incubated at 25 $^\circ\text{C}$, assessing both the solution without centrifugation and the supernatant after centrifugation (15 min, 13,200g; **Fig. 5b**). We added V ml of an I_β solution prepared by 52 h of incubation at 4 $^\circ\text{C}$ to 20 ml of a freshly prepared $\text{A}\beta_{1-40}$ solution at 25 $^\circ\text{C}$. The percentage of the seed was estimated from $V/(V + 20)$. Note that the concentration of $\text{A}\beta_{1-40}$ was unchanged by the addition of I_β because the I_β solution also contained 100 μM $\text{A}\beta_{1-40}$ in a monomer unit.

The ThT fluorescence increased in a sigmoidal manner after a lag time without seeding⁴⁷ for a mixed solution (**Fig. 5b**). Because higher temperature promotes fibril formation⁴⁶, the lag time observed at 25 $^\circ\text{C}$ (~ 3 h) was considerably shorter than that at 4 $^\circ\text{C}$ (~ 8 h). The ThT fluorescence for the supernatant sample suggested that the intermediate exists at 25 $^\circ\text{C}$ as a mixture with fibrils for 2–3 h at $t \approx 11$ h. Notably, at 5% and 13% seeding, the lag time was reduced in a concentration-dependent manner. In particular, the lag time was nearly truncated at 13% seeding. In addition, a rapid increase in ThT fluorescence was observed for the supernatant samples seeded with I_β

at both 5 and 13% (Fig. 5b). This observation confirms that I_β seeding promotes early formation of I_β in the course of misfolding. Thus, the data clearly demonstrate that adding I_β promotes fibril formation, suggesting that I_β is an on-pathway intermediate.

In this experiment, we expected some fluorescence at $t = 0$ from the seeded I_β (0.019 for 13%, 0.008 for 5%) on the basis of the simple dilution of I_β by monomeric $A\beta_{1-40}$ solution. By contrast, the fluorescence at $t = 0$ showed only a minimal increase (0.001 for 13% and 0.000 for 5%) at $t = 0$ h. This result suggests that I_β was in equilibrium with $I_{N\beta}$, which has no extended β -sheets, and that the equilibrium shifted toward $I_{N\beta}$ when I_β was seeded to the monomeric $A\beta_{1-40}$ because $[I_{N\beta}] \approx 0$ before the addition of I_β . Such a hypothesis is supported by the observation that adding I_β shortened the lag times required for β -sheet formation. If I_β were nearly completely dissolved into monomers, fibril formation would not be promoted in a manner dependent on the concentration of seeded I_β . It is also unlikely that fibrils or protofibrils were formed when I_β was added, because the addition of seed fibrils usually truncates a lag time and because early formation of I_β was observed in the seeding experiments. In the nucleation mechanism, this reduced fluorescence can be explained by the conversion of I_β back to nuclei aggregates after dilution. The absence of the ThT fluorescence clearly indicates, however, that these smaller aggregates lack fibril-like β -sheets detectable by ThT fluorescence. Thus, in either case, our fluorescence experiment suggests that $I_{N\beta}$ exists as an earlier intermediate before the appearance of I_β .

DISCUSSION

On the basis our structural and kinetic results, we propose the following molecular kinetic model (Fig. 5c). First, monomeric $A\beta_{1-40}$ molecules in random-coil conformations self-assemble into $I_{N\beta}$, an aggregate without amyloid-like β -sheet structures. Second, $I_{N\beta}$ assembles into I_β , a toxic spherical intermediate that is predominated by well-ordered parallel β -sheets. As shown in the fluorescence experiment, this step is likely to be reversible. Because $A\beta_{1-40}$ should be largely unstructured in a native monomer form, the early formation of $I_{N\beta}$ is consistent with reports of native-like small amyloid intermediates of $\beta 2$ microglobulin^{21,22}. Third, supramolecular reassembly of I_β produces protofibrils or fibrils. Our SSNMR analysis showed that the conformations of the fibril in the β -sheet regions are predefined by those of I_β . Therefore, it is highly likely that I_β and the fibril share a common parallel β -sheet structural motif, as shown in Figure 5c. Note that we have adopted our previous fibril structural model²⁹ of $A\beta_{1-40}$, in which two β -sheets are connected by a loop region, as a common motif between I_β and the fibril. A preliminary molecular modeling study has shown that supramolecular assembly in this organization of I_β yields a spherical morphology with a diameter of 16 nm and a molecular weight of 1–2 MDa (200–400 monomers), consistent with our observations in the glycerol gradient sedimentation assays (Supplementary Fig. 2).

At present, our suggested supramolecular structure of I_β remains a hypothetical model. For example, we also examined an alternative model comprising a single β -sheet structure without the loop region, which yielded a sphere of ~ 30 nm in diameter. Further studies are required to distinguish experimentally between these different models. In either model, packing of the common structural units is likely to be reorganized considerably in the structural transition from I_β to the fibril because kinetic properties, morphologies and toxicity differ markedly between I_β and the fibril despite the shared β -sheet conformations. In particular, the morphology of I_β lacks the apparent translational symmetry, which is observed in fibrils along the fiber axis. As in conversions to a native fold in protein folding,

rearrangements of side chain contacts are expected in the supramolecular structural conversion of I_β to the fibril. In future studies, we aim to address these structural issues by advanced SSNMR methods.

Our study highlights the importance of the structural characterization of late-stage amyloid intermediates, which has not been fully recognized in previous structural studies on amyloid misfolding. The high neurotoxicity of I_β suggests the possibility that structural conversion into β -sheets triggers neurotoxicity in amyloid misfolding, at least for $A\beta_{1-40}$. A study has suggested that the A11 antibody, which is targeted to earlier-stage spherical intermediates of $A\beta$, recognizes subfibrillar aggregates of various amyloid proteins including prion proteins and α -synuclein²⁷. Preliminary data obtained with the A11 antibody showed that I_β is recognized only weakly by A11 (Supplementary Fig. 2), implying that the surface structures of I_β differ from those of the earlier intermediates recognized by this antibody. More structural knowledge on other neurotoxic intermediates will provide understanding of the relationships between the neurotoxicity and molecular structures of I_β and those of various toxic amyloid intermediates. It is possible that the fibril-like β -sheet structure in I_β is shared by various toxic amyloid intermediates despite differences in the surface structures.

In summary, our SSNMR experiments and kinetic measurements have identified four biological and structural aspects of the structural evolution in amyloid misfolding of $A\beta$. First, we identified a highly neurotoxic amyloid intermediate species, I_β , which consists predominantly of well-ordered parallel β -sheet structures over the sequence. As compared with conventional structural analysis by solution NMR and X-ray crystallography of soluble proteins, SSNMR structural analysis of amyloid proteins usually provides fewer structural constraints^{29,31,32}. Nevertheless, our study has provided direct evidence of a late-stage diffusible amyloid intermediate that has well-defined β -sheet structures across the amino acid sequence with sequence specificity. The existence of this highly toxic amyloid intermediate with fibril-like β -sheet structures suggests that it will be feasible to design structural-based therapies to prevent or to detect amyloid formation at an early stage of Alzheimer's disease before plaques are formed¹.

Second, we have reported similarity between the molecular structures of I_β and those of the amyloid fibril. Thus, therapies targeting the β -sheet region in amyloid fibrils may also be effective against the amyloid intermediates. The higher neurotoxicity of I_β as compared with the fibril implies that the neurotoxicity of amyloid aggregates is influenced not only by conformations of the amyloid protein, but also by morphology or supramolecular structures of the aggregates. This result also shows that the parallel β -sheet structure in fibrils of $A\beta$ is defined at the stage of misfolding into I_β despite the morphological differences between the fibril and I_β . In this sense, I_β is a metastable intermediate stage that controls the profound conformational conversions toward the fibril in amyloid misfolding.

Third, our seeding experiment demonstrated that I_β is an on-pathway intermediate species that is in equilibrium with other earlier intermediates without extended β -sheet structures. Thus, removal of I_β is likely to suppress other earlier intermediate species through the equilibrium. Although it is still unclear whether I_β is the intermediate species that is pathologically responsible for Alzheimer's disease, the high neurotoxicity of I_β observed here implies that it is pathologically relevant.

Fourth, our studies demonstrated the possibility of evaluating time-dependent molecular structures in amyloid misfolding by SSNMR. A similar approach should be applicable to the misfolding of other amyloid-disease related proteins. Because self-assembly of amyloid

and other peptides has been useful for fabricating electronically or optically active nanomaterials^{48,49}, our approach may be useful for characterizing the structures and reaction pathways of nanoscale-assembled biomaterials.

METHODS

Sample preparation. Human A β_{1-40} peptide (NH₂-DAEFRHDSGYEVHHQKL VFFAEDVGSNKGAIIGLMVGGVV-COOH) was synthesized by standard solid-phase synthesis with an ABI 433 synthesizer. Unless otherwise noted, 100 μ M A β_{1-40} in 5 mM NaCl and 10 mM phosphate buffer was incubated at 4 °C. The A β_{1-40} solution was filtered before incubation with a 50-kDa-MWCO filter at 4 °C. During the incubation, the sample was gently mixed every 1–8 h before sampling an aliquot for ThT fluorescence measurements, which showed excellent reproducibility. For neurotoxicity assays and SSNMR, a spherical β -sheet amyloid intermediate was prepared by incubating 100 μ M A β_{1-40} for 50–52 h. To trap only the soluble species, the incubated A β_{1-40} solution was centrifuged at 13,200g for 15 min. The top 70% supernatant was collected, freeze-trapped in liquid nitrogen, and subsequently lyophilized for SSNMR. Although SSNMR analysis of a frozen solution is an option, here the low A β_{1-40} concentration (100 μ M) makes this option very challenging even in one-dimensional SSNMR. Thus, for sensitivity reasons, we chose to analyze the lyophilized samples. No extensive fibril formation or morphological changes were identified in the lyophilized I β sample by TEM (Supplementary Fig. 4) or by ThT fluorescence assay (Supplementary Fig. 5). A fibril sample was collected by further incubating the solution for 4–7 d.

MTT neurotoxicity assay. Toxicity was measured by a standard MTT assay²⁶, in which a reduction of 3-(4,5-dimethylthiazol-2-yl)-2,5-diphenyltetrazolium bromide (MTT) dye by the cells is optically measured as cell viability, as described⁵⁰. Rat pheochromocytoma PC12 cells were donated (see Acknowledgments) or purchased from ATCC. The cells were plated at a density of ~4,000 cells per well in 150 μ l of medium in a 96-well plate and incubated in a CO₂ incubator for 12 h at 37 °C before exposure to the toxin. Next, a 15- μ l aliquot of A β_{1-40} solution sampled at various incubation periods was added to the wells at the concentrations indicated, and the plate was incubated for an additional 4 h at 37 °C. The A β_{1-40} solution was diluted with medium if necessary. As a positive control, we added medium (15 μ l) to each well; a negative control sample was lysed by adding 0.1% Triton X-100 (BP151-100, Fisher) in place of A β_{1-40} solution⁵⁰. The cells were incubated for 4 h after the addition of MTT (CGD-1 kit, M-0283; Sigma-Aldrich) at a final concentration of 0.5 mg ml⁻¹. The cells were then lysed with 0.1 N HCl isopropanol, and the cellular reduction of MTT was optically quantified²⁶ (see Fig. 2 and the Supplementary Methods online for further details).

SSNMR. All SSNMR experiments were performed with a Varian Infinity-Plus SSNMR spectrometer with a 3.2-mm Varian T3 double- or triple-resonance magic angle spinning (MAS) probe at a ¹H frequency of 400.2 MHz, as described²⁵. The sample temperature was ~15 °C under MAS at 20 kHz. Patterns of cross peaks between directly connected ¹³C resonances (Fig. 3) provided reliable signal assignments on the basis of amino acid type⁴¹. All assignments are listed in Supplementary Table 1 online. Other details of the SSNMR experimental methods are given in the Supplementary Methods.

Other methods. A JEOL JEM-1220 TEM at an accelerating voltage of 120 kV was used for analysis of the morphologies of aggregated A β_{1-40} sampled at different incubation periods. Fluorescence measurements in the presence of ThT were performed on a Hitachi F-2000 fluorescence spectrometer at an excitation of 446 nm and emission of 482 nm, as described²⁵. The details of these methods are given in the Supplementary Methods.

Note: Supplementary information is available on the Nature Structural & Molecular Biology website.

ACKNOWLEDGMENTS

We thank M. Rasenick and J.-Z. Yu (University of Illinois at Chicago) for the PC-12 cells; L. Juarez and B. Lee for assistance with TEM studies and peptide synthesis, respectively; C. Bhardwaj, W. Cho and members of his group, and G. Fenteany for assistance with the neurotoxicity assay; R. Tycko for the structural

model of A β_{1-40} used in Fig. 4b and C. Jameson, T. Keiderling and W. Klein for suggestions. This work was supported in part by the Alzheimer's Association (NIRG 035123), the Dreyfus Foundation Teacher-Scholar Award program, the US National Science Foundation CAREER program (CHE 449952), and the National Institutes of Health RO1 program (AG028490).

Published online at <http://www.nature.com/nsmb/>

Reprints and permissions information is available online at <http://npg.nature.com/reprintsandpermissions>

- Selkoe, D.J. Cell biology of protein misfolding: the examples of Alzheimer's and Parkinson's diseases. *Nat. Cell Biol.* **6**, 1054–1061 (2004).
- Caughey, B. & Lansbury, P.T. Protofibrils, pores, fibrils, and neurodegeneration: Separating the responsible protein aggregates from the innocent bystanders. *Annu. Rev. Neurosci.* **26**, 267–298 (2003).
- Sunde, M. & Blake, C.C.F. From the globular to the fibrous state: protein structure and structural conversion in amyloid formation. *Q. Rev. Biophys.* **31**, 1–39 (1998).
- Dobson, C.M. Protein folding and misfolding. *Nature* **426**, 884–890 (2003).
- Bucciantini, M. *et al.* Inherent toxicity of aggregates implies a common mechanism for protein misfolding diseases. *Nature* **416**, 507–511 (2002).
- Lorenzo, A. & Yankner, B.A. β -amyloid neurotoxicity requires fibril formation and is inhibited by Congo red. *Proc. Natl. Acad. Sci. USA* **91**, 12243–12247 (1994).
- Walsh, D.M., Lomakin, A., Benedek, G.B., Condron, M.M. & Teplow, D.B. Amyloid β -protein fibrillogenesis—detection of a protofibrillar intermediate. *J. Biol. Chem.* **272**, 22364–22372 (1997).
- Lambert, M.P. *et al.* Diffusible, nonfibrillar ligands derived from A β_{1-42} are potent central nervous system neurotoxins. *Proc. Natl. Acad. Sci. USA* **95**, 6448–6453 (1998).
- Hoshi, M. *et al.* Spherical aggregates of β -amyloid (amylopherooid) show high neurotoxicity and activate tau protein kinase I/glycogen synthase kinase-3 β . *Proc. Natl. Acad. Sci. USA* **100**, 6370–6375 (2003).
- Nilsberth, C. *et al.* The 'Arctic' APP mutation (E693G) causes Alzheimer's disease by enhanced A β protofibril formation. *Nat. Neurosci.* **4**, 887–893 (2001).
- Lashuel, H.A. *et al.* Mixtures of wild-type and a pathogenic (E22G) form of A β 40 *in vitro* accumulate protofibrils, including amyloid pores. *J. Mol. Biol.* **332**, 795–808 (2003).
- Conway, K.A. *et al.* Acceleration of oligomerization, not fibrillization, is a shared property of both α -synuclein mutations linked to early-onset Parkinson's disease: Implications for pathogenesis and therapy. *Proc. Natl. Acad. Sci. USA* **97**, 571–576 (2000).
- McLean, C.A. *et al.* Soluble pool of A β amyloid as a determinant of severity of neurodegeneration in Alzheimer's disease. *Ann. Neurol.* **46**, 860–866 (1999).
- Lue, L.F. *et al.* Soluble amyloid β peptide concentration as a predictor of synaptic change in Alzheimer's disease. *Am. J. Pathol.* **155**, 853–862 (1999).
- Hsia, A.Y. *et al.* Plaque-independent disruption of neural circuits in Alzheimer's disease mouse models. *Proc. Natl. Acad. Sci. USA* **96**, 3228–3233 (1999).
- Walsh, D.M. *et al.* Naturally secreted oligomers of amyloid β protein potently inhibit hippocampal long-term potentiation *in vivo*. *Nature* **416**, 535–539 (2002).
- Lesne, S. *et al.* A specific amyloid- β protein assembly in the brain impairs memory. *Nature* **440**, 352–357 (2006).
- Kirkitadze, M.D., Condron, M.M. & Teplow, D.B. Identification and characterization of key kinetic intermediate in amyloid β -protein fibrillogenesis. *J. Mol. Biol.* **312**, 1103–1119 (2001).
- Krishnan, R. & Lindquist, S.L. Structural insights into a yeast prion illuminate nucleation and strain diversity. *Nature* **435**, 765–772 (2005).
- Liu, K., Cho, H.S., Lashuel, H.A., Kelly, J.W. & Wemmer, D.E. A glimpse of a possible amyloidogenic intermediate of transthyretin. *Nat. Struct. Biol.* **7**, 754–757 (2000).
- Jahn, T.R., Parker, M.J., Homans, S.W. & Radford, S.E. Amyloid formation under physiological conditions proceeds via a native-like folding intermediate. *Nat. Struct. Mol. Biol.* **13**, 195–201 (2006).
- Eakin, C.M., Berman, A.J. & Miranker, A.D. A native to amyloidogenic transition regulated by a backbone trigger. *Nat. Struct. Mol. Biol.* **13**, 202–208 (2006).
- Dobson, C.M. An accidental breach of a protein's natural defenses. *Nat. Struct. Mol. Biol.* **13**, 295–297 (2006).
- Chromy, B.A. *et al.* Self-assembly of A β (1–42) into globular neurotoxins. *Biochemistry* **42**, 12749–12760 (2003).
- Chimon, S. & Ishii, Y. Capturing intermediate structures of Alzheimer's β -amyloid, A β (1–40), by solid-state NMR spectroscopy. *J. Am. Chem. Soc.* **127**, 13472–13473 (2005).
- Shearman, M.S. Toxicity of protein aggregates in PC12 cells: 3-(4,5-dimethylthiazol-2-yl)-2,5-diphenyltetrazolium bromide assay. *Methods Enzymol.* **309**, 716–723 (1999).
- Kayed, R. *et al.* Common structure of soluble amyloid oligomers implies common mechanism of pathogenesis. *Science* **300**, 486–489 (2003).
- Lansbury, P.T. *et al.* Structural model for the β -amyloid fibril based on interstrand alignment of an antiparallel-sheet comprising a c-terminal peptide. *Nat. Struct. Biol.* **2**, 990–998 (1995).
- Petkova, A.T. *et al.* A structural model for Alzheimer's β -amyloid peptide fibrils based on experimental constraints from solid-state NMR spectroscopy. *Proc. Natl. Acad. Sci. USA* **99**, 16742–16747 (2002).
- Jaroniec, C.P., MacPhee, C.E., Astrof, N.S., Dobson, C.M. & Griffin, R.G. Molecular conformation of a peptide fragment of transthyretin in an amyloid fibril. *Proc. Natl. Acad. Sci. USA* **99**, 16748–16753 (2002).

31. Heise, H. *et al.* Molecular-level secondary structure, polymorphism, and dynamics of full-length α -synuclein fibrils studied by solid-state NMR. *Proc. Natl. Acad. Sci. USA* **102**, 15871–15876 (2005).
32. Ritter, C. *et al.* Correlation of structural elements and infectivity of the HET-s prion. *Nature* **435**, 844–848 (2005).
33. Benzinger, T.L.S. *et al.* Propagating structure of Alzheimer's β -amyloid(10–35) is parallel β -sheet with residues in exact register. *Proc. Natl. Acad. Sci. USA* **95**, 13407–13412 (1998).
34. Weliky, D.P. *et al.* Solid-state NMR evidence for an antibody-dependent conformation of the V3 loop of HIV-1 gp120. *Nat. Struct. Biol.* **6**, 141–145 (1999).
35. Igumenova, T.I. *et al.* Assignments of carbon NMR resonances for microcrystalline ubiquitin. *J. Am. Chem. Soc.* **126**, 6720–6727 (2004).
36. Castellani, F. *et al.* Structure of a protein determined by solid-state magic-angle-spinning NMR spectroscopy. *Nature* **420**, 98–102 (2002).
37. Lange, A. *et al.* Toxin-induced conformational changes in a potassium channel revealed by solid-state NMR. *Nature* **440**, 959–962 (2006).
38. Studelska, D.R., McDowell, L.M., Espe, M.P., Klug, C.A. & Schaefer, J. Slowed enzymatic turnover allows characterization of intermediates by solid-state NMR. *Biochemistry* **36**, 15555–15560 (1997).
39. Saito, H. Conformation-dependent ^{13}C chemical shifts: a new means of conformational characterization as obtained by high-resolution solid-state NMR. *Magn. Reson. Chem.* **24**, 835–852 (1986).
40. Spera, S. & Bax, A. Empirical correlation between protein backbone conformation and C- α and C- β C-13 nuclear-magnetic-resonance chemical shifts. *J. Am. Chem. Soc.* **113**, 5490–5492 (1991).
41. Ishii, Y. ^{13}C - ^{13}C dipolar recoupling under very fast magic angle spinning in solid-state NMR: Applications to distance measurements, spectral assignments, and high-throughput secondary-structure elucidation. *J. Chem. Phys.* **114**, 8473–8483 (2001).
42. Petkova, A.T. *et al.* Self-propagating, molecular-level polymorphism in Alzheimer's β -amyloid fibrils. *Science* **307**, 262–265 (2005).
43. Wishart, D.S., Bigam, C.G., Holm, A., Hodges, R.S. & Sykes, B.D. ^1H , ^{13}C and ^{15}N random coil NMR chemical shifts of the common amino acids. I. Investigations of nearest-neighbor effects. *J. Biomol. NMR* **5**, 67–81 (1995).
44. Cornilescu, G., Delaglio, F. & Bax, A. Protein backbone angle restraints from searching a database for chemical shift and sequence homology. *J. Biomol. NMR* **13**, 289–302 (1999).
45. Petkova, A.T., Yau, W.M. & Tycko, R. Experimental constraints on quaternary structure in Alzheimer's β -amyloid fibrils. *Biochemistry* **45**, 498–512 (2006).
46. Levine, H., III Quantification of β -sheet amyloid fibril structures with thioflavin T. *Methods Enzymol.* **309**, 274–284 (1999).
47. Naiki, H., Gejyo, F. & Nakakuki, K. Concentration-dependent inhibitory effects of apolipoprotein E on Alzheimer's β -amyloid fibril formation in vitro. *Biochemistry* **36**, 6243–6250 (1997).
48. Reches, M. & Gazit, E. Casting metal nanowires within discrete self-assembled peptide nanotubes. *Science* **300**, 625–627 (2003).
49. Zhang, S. Fabrication of novel biomaterials through molecular self-assembly. *Nat. Biotechnol.* **21**, 1171–1178 (2003).
50. Lambert, M.P. *et al.* Vaccination with soluble A β oligomers generates toxicity-neutralizing antibodies. *J. Neurochem.* **79**, 595–605 (2001).